RSC Advances

PAPER

View Article Online
View Journal | View Issue

Cite this: *RSC Adv.*, 2015, **5**, 69010

Covalent organic polymer framework with C–C bonds as a fluorescent probe for selective iron detection†

E. Özdemir, D. Thirion and C. T. Yavuz*

A new carbon–carbon bonded nanoporous polymer network was synthesized *via* efficient and catalyst free Knoevenagel-like condensation polymerization in near quantitative yields. The obtained polymer network, Covalent Organic Polymer – **COP-100** possesses strong fluorescent properties and designed solubility in polar aprotic solvents, which shows promise for use as a metal-sensing material in solution. **COP-100** exhibited high selectivity towards Fe^{2+} and Fe^{3+} in the presence of other common metal cations (Al^{3+}, Ag^{+}, Cd^{2+}, Co^{2+}, Cr^{3+}, Cu^{2+}, Hg^{2+}, Mg^{2+}, Mn^{2+}, Na^{+}, Ni^{2+}, Zn^{2+}) as the fluorescence of the polymer was significantly quenched even at very low concentrations. In the range from 2.5×10^{-6} to 2×10^{-4} M, a linear fluorescence emission response with equipment limited detection minimum of 2.13×10^{-7} M and 2.45×10^{-7} M for Fe^{2+} and Fe^{3+}, respectively, was observed. These results suggest that **COP-100** is a promising material as a selective fluorescence sensor for iron ions.

Received 5th June 2015
Accepted 6th August 2015

DOI: 10.1039/c5ra10697d

www.rsc.org/advances

Introduction

The widespread pollution in the environment stimulates intense research on the development of new functional materials with sensing and capture properties of the pollutants, such as metallic ions. Common fluorescent chemosensors for metallic ions are usually small molecules or conjugated polymers bearing strong chromophores.[1–3] Recently, network materials such as metal–organic frameworks (MOFs), microporous polymers were proposed as promising structures in sensor applications because of their structural tunability and superstructure heterogeneity.[4–8] A strong, functional, chemically robust framework that is immune to harsh environmental (exposure to acids, oxygen, UV, *etc.*) conditions is highly desired since sensing should not vary at each cycle or long-term exposure to the chemical feeds where the substrate to be detected exists.

Porous frameworks with targeted functionalities are commonly reported by using coupling reactions that are not necessarily designed to withstand chemical (*e.g.* water) or physical (*e.g.* heat) impacts.[9–16] In making the porous super structure, complexation by coordination chemistry of transition metals (such as in MOFs) or reversible click chemistries are often used. These methods lead to less than robust networks, showing vulnerability in durable applications.

One strategy to make a porous network stronger is to use the C–C bond in the formation of the polymer, albeit with the expense of losing chemical functionalities. The C–C bond forming coupling reactions that are employed so far were effective and able to give porous materials with very high surface area (*e.g.* Sonogashira, Yamamoto).[17,18] Nevertheless, they contained rare earth or reactive metal catalysts or harsh conditions with very poor atom economy (*e.g.* Friedel–Crafts).[19,20]

We have designed a C–C bonded network named **COP-100** (for covalent organic polymer) through a quick, effective and metal-free Knoevenagel-like condensation, where we both preserve functional groups and achieve C–C bonded, robust porous polymer. To the best of our knowledge this is the first effort in constructing robust porous polymers based on nitrile aldol condensation and one of the few that features fully C–C bonded framework.[21] By controlling the secondary, dehydration step, the obtained network showed slight solubility (up to 250 mg L^{-1}) in polar aprotic solvents such as DMF or DMSO, which is uncommon for polymeric networks.[22] This property allowed **COP-100** to be studied in solution, which is a major advantage in industrial applications such as membranes, compared to most of the insoluble porous polymeric networks. **COP-100** is strongly fluorescent and showed selective "turn-off" behaviour towards ferric and ferrous ions. The detection limit for these ions are among the best reported for polymer-based sensors.[23–26]

Korea Advanced Institute of Science and Technology (KAIST), Graduate School of Energy, Environment, Water, Sustainability (EEWS), Guseong Dong, Yuseong Gu, Daejeon 305-701, Korea. E-mail: yavuz@kaist.ac.kr

† Electronic supplementary information (ESI) available: Elemental analysis, thermogravimetric analysis, surface area measurements, absorption spectroscopy, fluorescence quenching titrations, and other materials. See DOI: 10.1039/c5ra10697d

Experimental

Materials

All materials and solvents were commercially available and used as received unless otherwise indicated. They included the following: 1,3,5-tris(bromomethyl)benzene (Sigma-Aldrich, 97%), potassium *tert*-butoxide (Acros, 98%), sodium cyanide (Samchun, 97%) and terephtaldehyde (Aldrich, 99%). THF was dried and collected from a Hansen Glass Contour Ultimate Solvent Purification 5 System.

Synthesis of network polymers

Synthesis of 2,2′,2″-(benzene-1,3,5-triyl) triacetonitrile (1). 1,3,5-tris(bromomethyl) benzene (3.02 g, 8.46 mmol) was dissolved in 30 mL tetrahydrofuran. Subsequently, 30 mL of saturated solution of sodium bicarbonate and sodium cyanide (4.17 g, 96.12 mmol) were added, followed by 30 mL water. The solution was stirred at room temperature for 48 h, and after which it was acidified with 1 M HCl until the pH was around 6. The precipitates were collected, washed with deionized water and dried in vacuum at 60 °C overnight to give the desired compound 1 as an off-white solid (1.65 g, 93.4%). ^{1}H NMR (300 MHz, $CDCl_3$, ppm): $\delta = 7.32$ (s, 3H, ArH), 3.81 (s, 6H, CH_2).

Synthesis of COP-100. Compound 1 (0.45 g, 2.31 mmol) and terephthaldehyde (0.47 mg, 3.50 mmol) were dissolved in THF (40 mL) at room temperature. Potassium *tert*-butoxide (1.10 g, 9.80 mmol) in THF was added and the mixture was stirred for 3 hours. Afterwards, the reaction mixture was poured into 200 mL of acidified ethanol (5% glacial AcOH). The resulting precipitates were separated by filtration, washed with ethanol and dried in vacuum at 60 °C overnight. **COP-100** was afforded as a pale yellow solid (0.88 g, 96%).

Characterizations

Liquid ^{1}H NMR was recorder on a Bruker AVANCE 300 MHz. $CDCl_3$ was used as a solvent and all chemical shifts are reported in ppm units with tetramethylsilane as internal standard. Solid state CP-MAS ^{13}C NMR spectra were recorded on a Bruker AVANCE 400WB spectrometer. Elemental analysis was performed at the KAIST Central Research Instrument Facility on a Thermo Scientific FLASH 2000 equipped with a TCD detector for carbon, nitrogen and hydrogen and on a Thermo Finnigan Flash EA 1112 for oxygen. Each experimental batch is measured twice and the elemental composition is given as a mean value of the two measurements. The reported composition of **COP-100** is the average of three separate experimental batches.

For the spectroscopic measurements, **COP-100** (25 mg) was stirred in DMF (100 mL) at 150 °C for 24 h to achieve full solubility. This solution was then diluted 25 times with DMF and used in the UV-Vis and fluorescence experiments. Metal ion solutions were prepared from the corresponding metal chlorides in 100 mL of DMF with a 10 mM concentration. Fluorescence emission spectra were recorded at 298 K unless otherwise specified. All titrations were carried out by gradually adding metal ion solutions. Each titration was repeated at least three times to get agreeable. **COP-100** solutions were excited at $\lambda_{exc} =$ 325 nm and their corresponding emission wavelength was monitored from $\lambda = 350$ nm to 625 nm. The fluorescence efficiency was calculated by $[(F_o - F)/F_o] \times 100\%$, where F_o and F are the fluorescence intensities of the **COP-100** solution in absence and presence of metal ion, respectively.

Photoluminescence data were collected on a luminescence spectrometer (Perkin Elmer LS-55). Photoluminescence decay times were measured by Time-Correlated Single Photon Count (TCSPC) on an Edinburgh Instruments FL920 using a 375 nm laser excitation. Decay times were fitted with the DecayFit 1.3 analysis software (http://www.fluortools.com). UV-Vis absorption spectra were measured with a Hach DR5000 UV-Vis spectrophotometer in quartz cells. Thermogravimetric analysis was performed on a Netzsch TG 209 F3 instrument by heating the samples up to 800 °C at a rate of 10 °C min^{-1} in nitrogen or air atmosphere. Infrared spectra (FT-IR) were recorded with a Jasco FT/IR-4100 type-A spectrometer using KBr pellets. Textural characterization of polymers was carried out from nitrogen adsorption isotherms using a Micromeritics 3FLEX accelerated surface area and porosimetry analyzer at 77 K or 87 K respectively. Measurements were performed on approximatively 100 mg of ground powders. Prior to measurement, samples were degassed at 423 K for 5 h under vacuum. The specific surface areas were derived from Brunauer–Emmett–Teller (BET) method. Average pore diameter data were determined by using the BJH desorption model.

The surface morphology of powder was examined by a scanning electron microscope (Hitachi S4800). Particle size was analyzed through dynamic light scattering on an ELS-Z2 (Otsuka Electronics, Japan). Samples were prepared as follows: 3 mg of **COP-100** were ground in a mortar and added into 6 mL of DMF. The mixture was sonicated for 30 minutes until the dispersion was homogeneous. The samples were measured at 25 °C.

Results and discussions

COP-100 was synthesized in one step from 1,3,5-benzenetriacetonitrile **1**[27] and commercially available terephthaldehyde **2** *via* Knoevenagel-like condensation (Fig. 1). The reaction proceeds smoothly at room temperature in the presence of potassium *tert*-butoxide in short reaction times (less than 3 hours) with almost quantitative yields (>95%). The resulting polymer network has been found to be slightly soluble in common polar aprotic solvents including dimethylformamide (DMF), dimethyl sulfoxide (DMSO), dimethylacetamide (DMAC) and *N*-methylpyrrolidone (NMP).

COP-100 has been studied by CP/MAS ^{13}C NMR, TGA, BET, SEM, DLS, FTIR, elemental analysis, UV-Vis and fluorescence

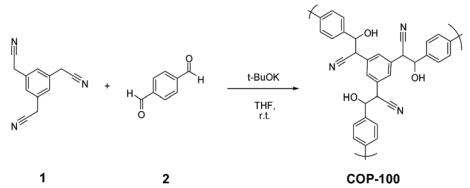

Fig. 1 Optimized synthesis conditions of polymer network **COP-100**.

spectroscopies in solution (for experimental details see Methods and ESI†). The maximum solubility of **COP-100** in DMF or DMSO of 0.25 mg mL^{-1} did not allow performing other liquid analysis (NMR, size exclusion chromatography) accurately.

A complete Knoevenagel condensation proceeds in two steps, first by deprotonation of an α-CN proton followed by nucleophile addition on the carbonyl and then, deprotonation of the second α-CN proton followed by dehydration. In a typical condensation reaction, especially when a conjugation is possible, dehydration of hydroxylated adduct is expected. This, however would lead to poly(phenylene vinylene) (PPV) structures, when employed in polymerization. Unfunctionalized PPVs are known to be insoluble and hard to process even in the linear forms.[28] For a soluble C–C bonded **COP-100** we deliberately optimized the reaction conditions, such as base, solvent and reaction temperature, in such a way that **COP-100** would not dehydrate (ESI Table S1†). We found that using a bulky base (*t*-BuOK), low temperature (r.t.) and aprotic solvent (THF) were ideal for fully hydroxylated **COP-100** where porosity is preserved. Furthermore, structures possessing both cyano and hydroxyl neighbouring units have been attracting targets in various fields of application.[29,30]

A possible explanation in the case of **COP-100** could be that the second deprotonation and following dehydration does not take place. The network structure is constructed very quickly and the bulky potassium *tert*-butylate is prevented from reaccessing the protons located inside the network. Less bulky bases are able to deprotonate the second proton inside the network, which is evidenced by the low oxygen content of the resulting polymers. The presence of hydroxyl groups makes **COP-100** slightly soluble in DMF and DMSO. Soluble polymer networks are known to allow membrane making, which have been attractive for CO_2 adsorption.[31]

Elemental analysis for **COP-100** (average of three separate batches) shows composition agreeing the formation of hydroxylated **COP-100** (Table 1, Fig. 2) rather than the conjugated form. Very minor dehydration due to the repetitive washes of dilute acetic acid in the ethanol may account for the slight difference of elemental distribution. It was reported that remaining moisture and air can also interfere with the oxygen content.[19–32]

The FT-IR spectrum of **COP-100** gave further insight in the chemical structure (Fig. 3a). The spectrum of **COP-100** shows the expected C–N stretching of the nitrile at 2221 cm^{-1} and several stretching related to the aromatic in the 1415–1698 cm^{-1} region and C–H in the 2925–3100 cm^{-1} region. But the FT-IR spectrum of **COP-100** also clearly shows a broad band around 3400 cm^{-1} characteristic of O–H stretching. The presence of hydroxyl groups is also confirmed by the C–O stretching at 1181 cm^{-1}.

Table 1 Elemental analysis of COP-100 and theoretical structures

	C	H	N	O
Fully dehydrated $C_{48}H_{24}N_6$	84.19	3.53	12.27	—
Hydroxylated $C_{48}H_{30}N_6O_6$	73.27	3.84	10.68	12.20
COP-100	75.70	5.13	8.03	11.14

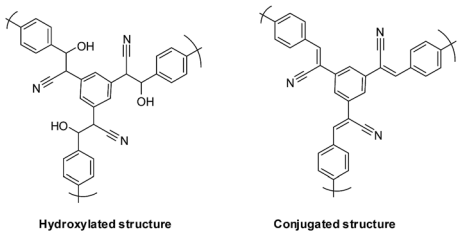

Fig. 2 Conjugated and hydroxylated structure of COP-100.

The solid state NMR spectrum of **COP-100** (Fig. 3b) shows a broad central region between 120 and 150 ppm containing the signals of all aromatic and nitrile carbons. Little residual peaks of unreacted aldehyde and CH_2CN can be found around 176 ppm and 25 ppm respectively. The peak at 95 ppm, attributed to =CCN is weak in intensity, which means that there are only few alkene bonds in the **COP-100**. The spectrum of **COP-100** shows also the presence of signals at 71 and 50 ppm. Those signals can be attributed to CHOH and CHCN, respectively.

The specific surface area and pore size distribution of the network structure were derived from nitrogen adsorption desorption isotherms by BET and BJH desorption model, respectively. The results revealed that surface area and pore size distribution can be tuned by varying synthesis conditions. The BET surface area for **COP-100** varied from 4.3 to 82.3 $m^2\ g^{-1}$ in conjunction with the base/solvent couple. The highest specific surface area was obtained when *t*-BuOK was used (ESI Table S2†). Adsorption–desorption isotherms of **COP-100** resemble type IIb with H3 hysteresis loop according to IUPAC classification.[33] Type IIb isotherms are aggregates of plate like particles, possessing non-rigid slit-shaped pores. The isotherm shapes show that **COP-100** is dominantly mesoporous that extends into the macropore region with negligible micropores. The porosity of the material was further confirmed by the BJH pore size distribution data with average pore diameters of 27 nm. The morphology of **COP-100** was examined by scanning electron microscopy (SEM). As shown in Fig. 4, interparticle voids that connect to the surface can be seen clearly. The total volume of these open pores depends on the size of the individual particles. The prediction of the average size of the particles from SEM images is not possible, therefore we further investigated the particle size distribution by dynamic light scattering (DLS), as presented in Fig. S1.† DLS analysis of **COP-100** shows bimodal distribution of particle size. The main particle size distribution is centered on a diameter of 1000 nm and a second smaller region is centered on 11 500 nm. This is reflected in the high polydispersity index of 0.42–0.47. The particle size distribution is consistent with the SEM images of **COP-100**.

Thermogravimetric analysis of **COP-100** was performed up to 800 °C at a heating rate of 10 °C min^{-1} in air and nitrogen environment (ESI Fig. S2†). Nanoporous organic polymers especially fully aromatic ones have been reported to have thermal stability often above 300 °C.[34,35] **COP-100** shows a gradual and slow mass loss of 6% from 100 °C to 300 °C. Between 330 °C and 350 °C the mass loss increases significantly which can be attributed to the decomposition of the structure.

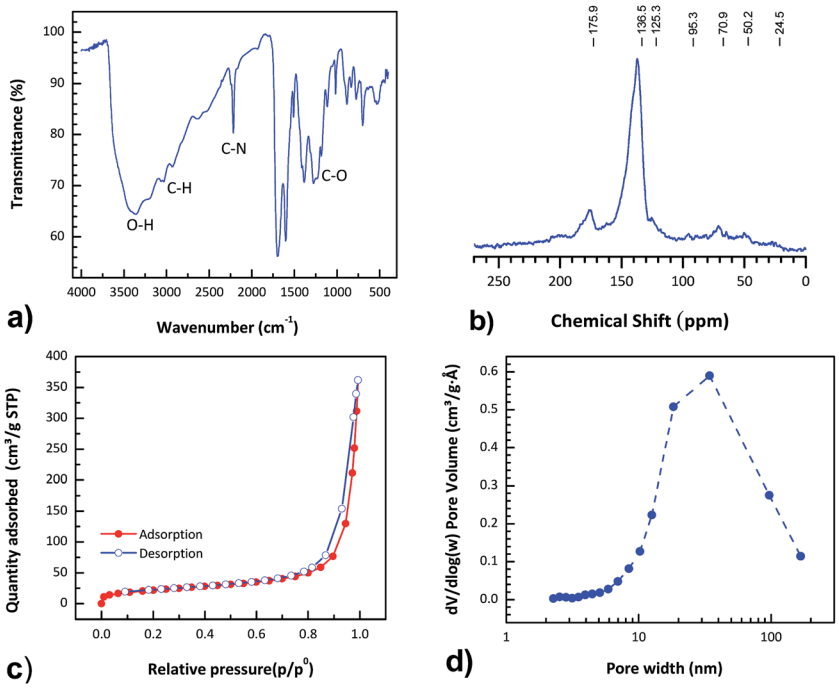

Fig. 3 (a) FT-IR and (b) CP-MAS ^{13}C spectra of **COP-100**. (c) Nitrogen sorption isotherms measured at 77 K and (d) BJH pore size distribution.

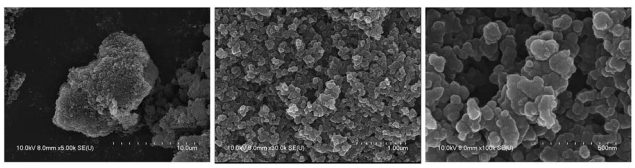

Fig. 4 SEM images of **COP-100** with various magnification.

COP-100 has been studied in UV-visible and fluorescence spectroscopy in solution in DMF at a concentration of 10 μg mL^{-1}. The UV-visible spectrum of **COP-100** is a single absorption band with a maximum at 323 nm. The optical band gap determined from the edge of the absorption (428 nm) is 2.89 eV (Fig. 5a). This high value, compared to cyano containing PPV structures,[36] can be explained by a short conjugation length because the structure of **COP-100** is not fully conjugated. It is important to note that the synthesis of **COP-100** is reproducible as proven by chemical and porosity characterizations, and that the obtained structure is always consistent. The emission spectrum of **COP-100** is also broad and structureless, with a maximum at 420 nm and a shoulder at 484 nm. The Stokes shift of 715 cm^{-1} is strong (Fig. 5a). These can be probably be explained by the compact network structure of **COP-100** which leads to intramolecular interactions between aryl units.

In order to investigate the potential application of **COP-100** as a sensing material, titration spectra with a large panel of metal ions have been performed. The UV-visible absorption spectra of **COP-100** do not show any influence by metal cations and therefore the analysis will be focused on the fluorescence responses only (see Fig. S3 in ESI† for UV-Vis spectra).

The fluorescence spectral studies of **COP-100** were performed in the presence of different metal ions such as Al^{3+}, Ag^{+}, Cd^{2+}, Co^{2+}, Cr^{3+}, Cu^{2+}, Fe^{2+}, Fe^{3+}, Hg^{2+}, Mg^{2+}, Mn^{2+}, Na^{+}, Ni^{2+}, Zn^{2+}. Fig. 5b shows the corresponding difference of fluorescence intensity of **COP-100** in DMF (10 μg mL^{-1}) after addition of different metal ions (100 μM). Except the iron cations, no

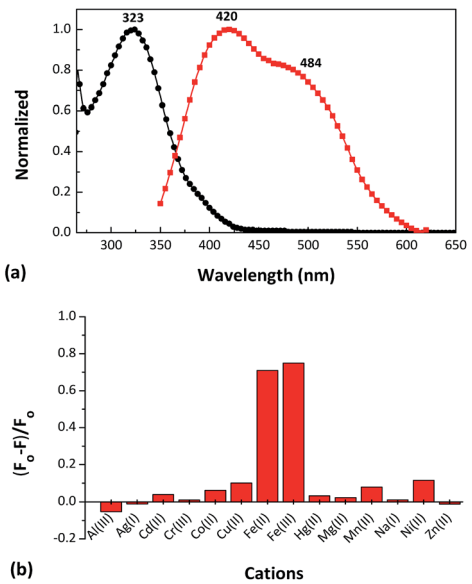

Fig. 5 (a) Normalized UV-visible spectrum (black) and fluorescence spectrum (red, excitation at 323 nm) of **COP-100** in DMF (b) fluorescence intensity difference of **COP-100** (10 μM) after addition of Al(III), Ag(I), Cd(II), Co(II), Cr(III), Cu(II), Fe(II), Fe(III), Hg(II), Mg(II), Mn(II), Na(I), Ni(II), Zn(II) (100 μM) in DMF solution. F_o and F are the fluorescence intensities in the absence and presence of metal ions respectively.

significant loss of intensity was observed in the presence of most major metal ions. To examine the selective competition quenching response of **COP-100**, a fixed concentration of metal fluorescence emission spectra were recorded before and after the adding of interferents. Selective competition quenching of **COP-100** upon the addition of metal ions is shown in Fig. 7a. Upon the addition of Fe^{2+} or Fe^{3+} led to a significant quenching (63.4 and 70.3%, respectively) of the original fluorescence intensity. When both Fe^{2+} and Fe^{3+} were added to **COP-100**, the quenching was increased to 82%. On the other hand, addition of the other metal ions (**A**) gave negligible changes in the fluorescence intensity (7.6%).

Fluorescence of **COP-100** solutions and its quenching by Fe^{3+} was performed at pH values ranging from 1 to 14 (see Fig. 7b). **COP-100** shows very similar fluorescence from pH $\sim$ 1 to $\sim$7.5. At these pH values, the quenching efficiency is almost the same (32% to 40% respectively with an addition of 12.5 μM Fe^{3+}). At pH $\sim$ 10.5 and $\sim$14 however, the fluorescence of **COP-100** is diminished by 24% and the quenching efficiency drops to 7–8% (12.5 μM Fe^{3+}). **COP-100** is more efficiently used as iron sensing material in acidic to neutral conditions but is less usable in basic conditions. All following fluorescence experiments were performed at pH $\sim$ 7.5 (DMF).

In order to quantify the detecting behaviour of **COP-100** towards ferric and ferrous cations, fluorescence titration experiments were conducted. The fluorescence spectrum of **COP-100** showed "turn-off" responses even when adding small concentrations of iron in DMF. Increasing the concentration

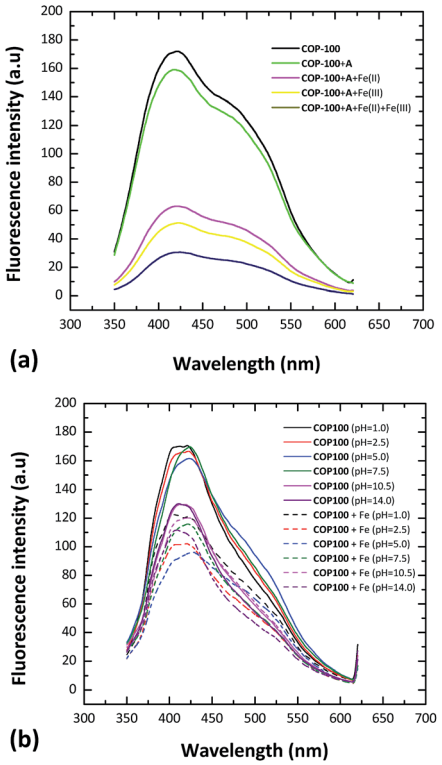

Fig. 7 (a) Selective competition quenching of **COP-100** by various metal ions **A** (**A** = Al^{3+} + Ag^{+} + Cd^{2+} + Co^{2+} + Cr^{3+} + Cu^{2+} + Hg^{2+} + Mg^{2+} + Mn^{2+} + Na^{+} + Ni^{2+} + Zn^{2+}) and iron cations (Fe^{2+}, Fe^{3+}). (b) Fluorescence of **COP-100** at pH 1–14 with or without Fe^{3+}.

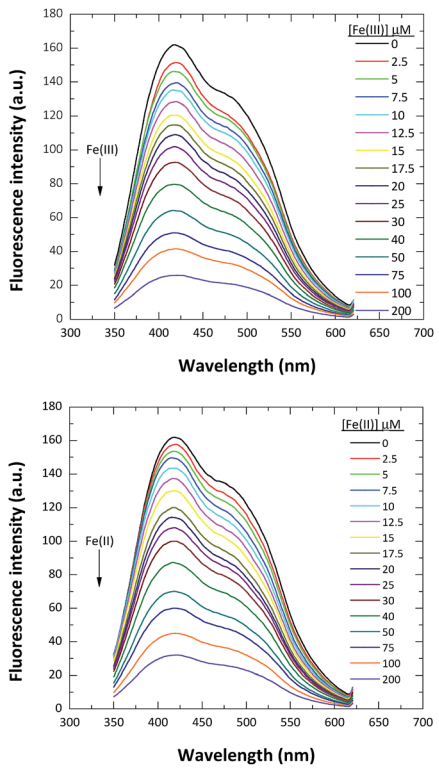

Fig. 6 Fluorescence titration of **COP-100** (10 μg mL^{-1}) with incremental addition of Fe^{2+} and Fe^{3+} in DMF (exc. 325 m).

of iron ion concentrations from 2.5 × 10^{-6} to 2 × 10^{-4} M resulted in sharp decrease of fluorescence intensity as shown in Fig. 6. The Stern–Volmer plot of the titration curves of **COP-100** shows a good linear relationship and low standard errors for ferrous and ferric ions concentration (see Fig. S4 in ESI†). Standard deviations of the fits are characterized by a good correlation coefficient. The quenching constant was calculated from slope of the fitted line as 2.58 × 10^4 for Fe(II) and 2.97 × 10^4 for Fe(III). The limit of detection was found as 2.45 × 10^{-7} M for Fe(II) and 2.13 × 10^{-7} M for Fe(III). The linear Stern–Volmer plot indicates that only one kind of quenching occurs. Common "turn-off" chemosensors work on the principle of static quenching through formation of non-emissive complexes.[23,37]

As the ground state of **COP-100** is unaffected by the presence of iron cations, it is unlikely that the quenching mechanism in this case is static. To verify this hypothesis, fluorescence decay times of **COP-100** solutions in the presence of different concentration of Fe(III) have been measured (see ESI Fig. S5†). The decay times of all tested solutions can be fitted by similar triple exponential functions, but the average decay time is diminishing with increased iron concentration, from 1.03 ns for **COP-100** to 0.67 ns for **COP-100** quenched by a 50 μM Fe(III) (see ESI Table S3†). As the decay times are diminishing, the nature of the fluorescent entities in the solution is changing. Hence the quenching of **COP-100** can most likely be attributed to collisional quenching. In order to fully understand the nature of the

three fluorescent entities from **COP-100** and the quenching mechanism, further work is currently performed in our group.

Conclusions

In conclusion, a new carbon–carbon bonded porous network polymer, **COP-100**, was successfully designed and synthetized *via* quick, efficient and metal-free procedure. The reaction conditions were optimized to enhance solubility of **COP-100** in polar aprotic solvents. **COP-100** exhibited high selectivity towards Fe^{2+} and Fe^{3+} in the presence of other common metal cations (Al^{3+}, Ag^{+}, Cd^{2+}, Co^{2+}, Cr^{3+}, Cu^{2+}, Hg^{2+}, Mg^{2+}, Mn^{2+}, Na^{+}, Ni^{2+}, Zn^{2+}) as the fluorescence of the polymer was significantly quenched even at very low concentrations. In the range from 2.5×10^{-6} to 2×10^{-4} M, a linear fluorescence emission response with equipment limited detection minimum of 2.13×10^{-7} M and 2.45×10^{-7} M for Fe^{2+} and Fe^{3+}, respectively, was observed. These results suggest that **COP-100** is a promising material as a selective fluorescence sensor for iron ions.

Acknowledgements

We acknowledge the financial support by grants from Basic Science Research Program (2013R1A1-A1012998), and IWT (NRF-2012-C1AAA001-M1A2A2026588), funded by National Research Foundation of Korea (NRF) under the Ministry of Science, ICT & Future Planning of Korean government.

References

1 H. N. Kim, Z. Guo, W. Zhu, J. Yoon and H. Tian, *Chem. Soc. Rev.*, 2011, **40**, 79–93.
2 Y. Jeong and J. Yoon, *Inorg. Chim. Acta*, 2012, **381**, 2–14.
3 B. Wang and E. V. Anslyn, *Chemosensors: Principles, Strategies and Applications*, Wiley, 2011.
4 L. E. Kreno, K. Leong, O. K. Farha, M. Allendorf, R. P. van Duyne and J. T. Hupp, *Chem. Rev.*, 2011, **112**, 1105–1125.
5 X. Li, H. Xu, F. Kong and R. Wang, *Angew. Chem., Int. Ed.*, 2013, **52**, 13769–13773.
6 Y. Yuan, H. Ren, F. Sun, X. Jing, K. Cai, X. Zhao, Y. Wang, Y. Wei and G. Zhu, *J. Phys. Chem. C*, 2012, **116**, 26431–26435.
7 L. Sun, Z. Liang, J. Yu and R. Xu, *Polym. Chem.*, 2013, **4**, 1932–1938.
8 X. Liu, Y. Xu and D. Jiang, *J. Am. Chem. Soc.*, 2012, **134**, 8738–8741.
9 L. G. Beauvais, M. P. Shores and J. R. Long, *J. Am. Chem. Soc.*, 2000, **122**, 2763–2772.
10 M. Eddaoudi, J. Kim, N. Rosi, D. Vodak, J. Wachter, M. O'Keeffe and O. M. Yaghi, *Science*, 2002, **295**, 469–472.
11 A. M. M. El-Betany and N. B. McKeown, *Tetrahedron Lett.*, 2012, **53**, 808–810.
12 R. Guliyev, A. Coskun and E. U. Akkaya, *J. Am. Chem. Soc.*, 2009, **131**, 9007–9013.
13 S. Kitagawa and R. Matsuda, *Coord. Chem. Rev.*, 2007, **251**, 2490–2509.
14 L. J. Murray, M. Dinca, J. Yano, S. Chavan, S. Bordiga, C. M. Brown and J. R. Long, *J. Am. Chem. Soc.*, 2010, **132**, 7856–7857.
15 Y. Takashima, V. M. Martinez, S. Furukawa, M. Kondo, S. Shimomura, H. Uehara, M. Nakahama, K. Sugimoto and S. Kitagawa, *Nat. Commun.*, 2011, **2**, 168.
16 Z. Kahveci, T. Islamoglu, G. A. Shar, R. Ding and H. M. El-Kaderi, *CrystEngComm*, 2013, **15**, 1524–1527.
17 J.-X. Jiang, F. Su, A. Trewin, C. D. Wood, N. L. Campbell, H. Niu, C. Dickinson, A. Y. Ganin, M. J. Rosseinsky, Y. Z. Khimyak and A. I. Cooper, *Angew. Chem., Int. Ed.*, 2007, **46**, 8574–8578.
18 J. Schmidt, M. Werner and A. Thomas, *Macromolecules*, 2009, **42**, 4426–4429.
19 C. F. Martin, E. Stockel, R. Clowes, D. J. Adams, A. I. Cooper, J. J. Pis, F. Rubiera and C. Pevida, *J. Mater. Chem.*, 2011, **21**, 5475–5483.
20 H. Lim, M. C. Cha and J. Y. Chang, *Polym. Chem.*, 2012, **3**, 868–870.
21 Y.-C. Zhao, D. Zhou, Q. Chen, X.-J. Zhang, N. Bian, A.-D. Qi and B.-H. Han, *Macromolecules*, 2011, **44**, 6382–6388.
22 Q. Liu, Z. Tang, M. Wu and Z. Zhou, *Polym. Int.*, 2014, **63**, 381–392.
23 S. Huang, P. Du, C. Min, Y. Liao, H. Sun and Y. Jiang, *J. Fluoresc.*, 2013, **23**, 621–627.
24 I. Grabchev, S. Sali, R. Betcheva and V. Gregoriou, *Eur. Polym. J.*, 2007, **43**, 4297–4305.
25 Y. Hu, B. Wang and Z. Su, *Polym. Int.*, 2008, **57**, 1343–1350.
26 T. Palanché, F. Marmolle, M. A. Abdallah, A. Shanzer and A. M. Albrecht-Gary, *J. Biol. Inorg. Chem.*, 1999, **4**, 188–198.
27 M. Kathiresan, L. Walder, F. Ye and H. Reuter, *Tetrahedron Lett.*, 2010, **51**, 2188–2192.
28 R. Y. Li, Y. J. Mo, R. Shi, P. Li, C. Y. Li, Z. J. Wang, X. Wang and S. B. Li, *Monatsh. Chem.*, 2014, **145**, 85–90.
29 P. Kisanga, D. McLeod, B. D'S and J. Verkade, *J. Org. Chem.*, 1999, **64**, 3090–3094.
30 A. Goto, K. Endo, Y. Ukai, S. Irle and S. Saito, *Chem. Commun.*, 2008, 2212–2214.
31 X. Zhu, C. Tian, S. Chai, K. Nelson, K. S. Han, E. W. Hagaman, G. M. Veith, S. M. Mahurin, H. Liu and S. Dai, *Adv. Mater.*, 2013, **25**, 4152–4158.
32 Y. Yang, Q. Zhang, S. Zhang and S. Li, *RSC Adv.*, 2014, **4**, 5568–5574.
33 F. Rouquerol, J. Rouquerol and K. S. W. Sing, *Adsorption by powders and porous solids: Principles, methodology, and applications*, Academic Press, San Diego, 1999.
34 H. A. Patel, F. Karadas, J. Byun, J. Park, E. Deniz, A. Canlier, Y. Jung, M. Atilhan and C. T. Yavuz, *Adv. Funct. Mater.*, 2013, **23**, 2270–2276.
35 R. Dawson, D. J. Adams and A. I. Cooper, *Chem. Sci.*, 2011, **2**, 1173–1177.
36 J. Liao and Q. Wang, *Macromolecules*, 2004, **37**, 7061–7063.
37 L. Li, N.-F. She, Z. Fei, P.-K. So, Y.-Z. Wang, L.-P. Cao, A.-X. Wu and Z.-P. Yao, *J. Fluoresc.*, 2011, **21**, 1103–1110.